

Results of Multiple Tracer Injections into Fractures in the EGS Collab Testbed-1

Ghanashyam Neupane¹, Earl D. Mattson², Mitchell A. Plummer¹, Robert K. Podgorney¹, and the EGS Collab Team³

¹Idaho National Laboratory, Idaho Falls, ID 83415

²Mattson Hydrology, LLC., Idaho Falls, ID 83402

Ghanashyam.Neupane@inl.gov

Keywords: EGS, fracture characterization, hydraulic fractures, field tracer test

ABSTRACT

The EGS Collab project constructed an intermediate scale (~10-20 m) testbed at the 4850 level of the Stanford Underground Research Facility (SURF) in South Dakota for testing and validating fracture stimulation and flow/transport models. This testbed consists of eight ~200 ft (~60 m) HQ-diameter (9.6 cm) boreholes that are drilled into the crystalline rocks of the Poorman Formation from the West Access Drift tunnel. Of the eight boreholes, one borehole is used as an injection/stimulation well, while another sub-parallel borehole located about 10 m away from the injection well is used as a production well, and rest of the other boreholes are used as geophysical/fluid sampling monitoring wells. Hydraulic stimulation activities were conducted at three locations along the injection hole in an attempt to create direct fracture connections to the production hole. A flow system has been established between injection and production boreholes through a set of hydraulically stimulated fractures propagated from a notch located at 164 ft in the injection hole. Although we planned for a single production well, a set of natural fractures in the testbed is believed to have intersected the stimulated hydraulic fractures and provided additional flow paths for water to be transported to the drift through multiple monitoring boreholes and weep zones. As the flow tests continued after stimulation activities, single or a combination of two or three producers become dominant producers at different times, mostly as a response to intersection of hydraulic fracture and testbed wells, activation of natural fractures and making new leak points to the monitoring wells, resealing of leaky wells, and so on. Since late October 2018, multiple tracers were injected into the fracture system at the 164 ft location that involves both stimulated and natural fractures, and tracers were recovered from multiple locations in nearby wells and weep. The cumulative water recoveries over the time have ranged from 50 to 90%; however, the injected tracer recoveries from various production sources are much less (ranging from a few percentages to 38%). Changes in water/tracer recoveries, shifting of major producing wells from one well to the others, and other observations (e.g., microseismic, electric resistivity tomography, etc.) indicate a testbed that has undergone several changes since October 2018. In this paper, we present tracer recovery data accumulated during several tracer campaigns, provide conceptual testbed flow pathways, and provide observations that suggest an evolutionary nature of fracture volume and fracture geometry in the testbed.

1. INTRODUCTION

The United States Geological Survey (USGS) estimates an enormous indigenous renewable energy potential from enhanced or engineered geothermal systems (EGS) in the US (Williams et al., 2008). To realize this potential, the US Department of Energy (DOE) Geothermal Technologies Office (GTO) has initiated a series of EGS programs including Frontier Observatory for Research in Geothermal Energy (FORGE). The FORGE is geared towards creating a full-scale field laboratory with a focus on testing and validating technologies to improve EGS reservoir access, creation, and sustainability (Moore et al., 2019). As a bridge to the FORGE initiative, the DOE-GTO is also funding a research project – EGS Collab Project– to create an intermediate-scale reservoir in underground facility that provides a more accessible reservoir for refining our understanding of rock mass response to stimulation, testing novel monitoring tools, and validating thermal- hydrological- mechanical- chemical (THMC) modeling approaches (Dobson et al., 2017; Kneafsey et al., 2019; White et al., 2019; White and Fu, 2020). Testbed for this project is developed at the Sanford Underground Research Facility

³The Collab Team: J. Ajo-Franklin, T. Baumgartner, K. Beckers, D. Blankenship, A. Bonneville, L. Boyd, S. Brown, S.T. Brown, J.A. Burghardt, T. Chen, Y. Chen, K. Condon, P.J. Cook, D. Crandall, P.F. Dobson, T. Doe, C.A. Doughty, D. Elsworth, J. Feldman, A. Foris, L.P. Frash, Z. Frone, P. Fu, K. Gao, A. Ghassemi, H. Gudmundsdottir, Y. Guglielmi, G. Guthrie, B. Haimson, A. Hawkins, J. Heise, M. Horn, R.N. Horne, J. Horner, M. Hu, H. Huang, L. Huang, K.J. Im, M. Ingraham, R.S. Jayne, T.C. Johnson, B. Johnston, S. Karra, K. Kim, D.K. King, T. Kneafsey, H. Knox, J. Knox, D. Kumar, K. Kutun, M. Lee, K. Li, Z. Li, R. Lopez, M. Maceira, P. Mackey, N. Makedonska, C.J. Marone, E. Mattson, M.W. McClure, J. McLennan, T. McLing, C. Medler, R.J. Mellors, E. Metcalfe, J. Miskimins, J. Moore, C.E. Morency, J.P. Morris, S. Nakagawa, G. Neupane, G. Newman, A. Nieto, C.M. Oldenburg, W. Pan, T. Paronish, R. Pawar, P. Petrov, B. Pietzyk, R. Podgorney, Y. Polsky, J. Pope, S. Porse, B.Q. Roberts, M. Robertson, W. Roggenthen, J. Rutqvist, D. Rynders, H. Santos-Villalobos, M. Schoenball, P. Schwering, V. Sesity, C.S. Sherman, A. Singh, M.M. Smith, H. Sone, F.A. Soom, P. Sprinkle, C.E. Strickland, J. Su, D. Templeton, J.N. Thomle, C. Ulrich, N. Uzunlar, A. Vachapampil, C.A. Valladao, W. Vandermeer, G. Vandine, D. Vardiman, V.R. Vermeul, J.L. Wagoner, H.F. Wang, J. Weers, N. Welch, J. White, M.D. White, P. Winterfeld, T. Wood, S. Workman, H. Wu, Y.S. Wu, Y. Wu, E.C. Yildirim, Y. Zhang, Y.Q. Zhang, Q. Zhou, M.D. Zoback

(SURF), a dedicated underground research facility that uses the extensive network of tunnel systems developed over a century of gold mining activities as Homestake Gold Mine, in Lead, South Dakota (Heise, 2015; Kneafsey et al., 2019, 2020).

Over the last few years, multiphase hydraulic fracturing activities, several interwell flow tests, and a series of fracture characterization tests (e.g., chemical and thermal tracers) were conducted in the testbed located almost 1.5 km below the ground surface (Ulrich et al., 2018; Hunag et al., 2019; Kneafsey et al., 2019; White et al., 2019; Singh et al., 2019). In our previous efforts (e.g., Mattson et al., 2019a, b), we presented earlier tracer tests results. In this paper, we present tracer recovery data accumulated from April until November 2019. As the testbed has undergone several changes, we provide conceptual testbed flow pathways during several tracer tests and include simple tracer analyses that relate tracer data to the evolutionary nature of fracture volume and fracture geometry in the testbed.

2. EGS COLLAB TESTBED-1

The testbed is located on the western rib of the West Access Drift of the 4850 Level (4850 feet below ground surface), nearby Governor’s Corner (Figure 1). The testbed is accessible via Yates Shaft and Ross Shaft. Once cage downed to 4850 level, the site can be reached directly through the West Access Drift or via the East Drift and South Drift. The site is well ventilated and provided with electricity, internet, running water, drainage, and so on.

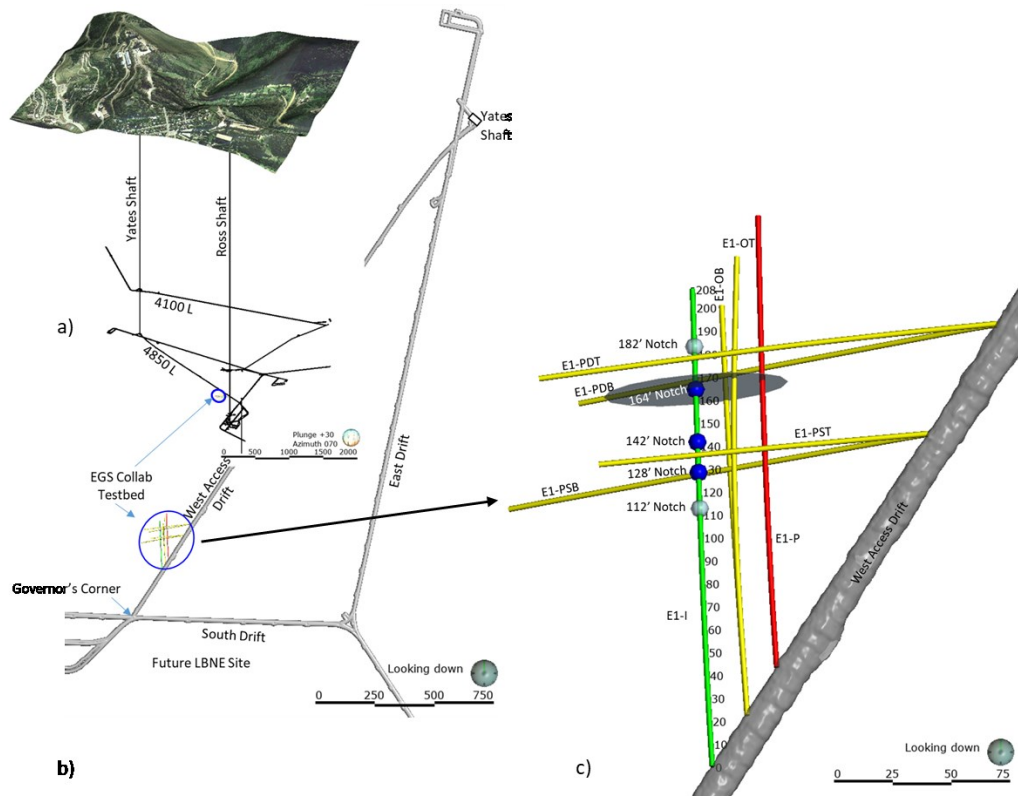


Figure 1. a) EGS Collab Testbed-1 at SURF is located about 1.5 km below ground surface at Sanford Underground Research Facility (SURF). b) The testbed is developed on the 4850 level along the West Access Drift, near Governor’s Corner. c) The testbed has 8 boreholes; six of them (yellow lines) are used as monitoring wells, one borehole (green line) is used as an injection/stimulation well, and the remaining one (red line) is used as a production well. The three dark blue spheres along E1-I are stimulation notches where some stimulation works have been conducted, and the two light blue spheres are additional notches that have yet to be stimulated. The large disk at 164 notch represents the expected hydraulic fracture radiating from the notch.

The EGS Collab Experiment-1 (E1) testbed consists of eight HQ-diameter (9.6 cm), continuously cored sub-horizontal holes with nominal length of about 200 ft (Figure 3a). Each hole was steel cased to a depth of 20 ft from top (collar). Six of the boreholes (E1-OT, E1-OB, E1-PST, E1-PSB, E1-PDT, and E1-PDB) are heavily equipped with various equipment for seismic, temperature, electrical resistivity monitoring (Figure 3b), and grouted with a mixture of ground blast furnace slag, ground pumice, and Portland cement. The remaining two holes (E1-I and E1-P) are remained open and being used as stimulation and production wells. Five notches were created at different depths along the E1-I to facilitate stimulation and guide initiate intended hydraulic fracturing.

The layout of the testbed boreholes was designed to create stress-field controlled hydraulic fracture(s) and to provide maximum opportunity to characterize/monitor fracturing event(s) (Knox et al., 2017). The injection well (E1-I) and production well (E1-P) were drilled (nominal azimuth = 356° and inclination = 12°) approximately parallel with the trend of minimum horizontal stress (trend = 003°

and plunge = 9.3°) in the area (which was previously determined at a nearby kISMET testbed (Oldenburg et al., 2016) with intended hydraulic fracture striking along the maximum horizontal stress with a dip of ~ 81.7° (as depicted by the disk at 164-notch in Figure 1c). The two boreholes (E1-OT and E1-OB) are designed as nearby monitoring holes orthogonally intersecting the intended hydraulic fracture. Other four monitoring holes (E1-PST, E1-PSB, E1-PDT, and E1-PDB) are designed as being shallow and deep wells that are intended to be parallel with the hydraulic fracture (White et al., 2017; Knox et al., 2017).

3. TRACER TESTS

3.1 Target Zone

Several tracer injection campaigns were completed at the testbed since October 2018 to November 2019. Non-reactive (conservative), reactive (sorbing), and thermally degrading tracers (Table 1) were injected, either exclusively or in combination, and their recovery from multiple producers were collected and analyzed. Each tracer test injected at 164-notch and targeted characterization of hydraulic fracture(s) that was might have connected to natural fractures providing flow paths to E1-P (at multiple depths), several monitoring holes, and drift E1-I. The activities to create hydraulic fracture(s) at 164-notch was commenced during May 22-25, 2018 (White et al., 2019). Previously, we showed that the hydraulic fracture(s), two natural fracture zones, (OT-P Connector and PDT-OT Connector), E1-P, and at least 3 monitoring holes (E1-OT, E1-PST, and E1-PDT) were involved in defining dominant flow paths at one time or the other during the flow tests (Neupane et al., 2019, Figure 2). Also, the Shallow fracture zone/weep depicted in Figure 2 is indirectly served as a flow path during flow test at 164-notch. After the top section of the E1-OT was sealed, water leaked to this hole at depth moved up and diverted into the Shallow fracture zone, and ultimately seeped to the drift as a weep near E1-P.

3.2 Tracer Injection

All tracer tests were conducted with a nominal injection rate of 400 mL/min. Most of the time since late October 2018, the testbed is under constant flow regime with some interruptions. When there was an interruption in injection prior to a tracer test, a steady flow regime was established before injection of tracer solution. Since early May 2019, the testbed was subjected to a chilled water injection although there have been some brief durations when the regular mine water was injected because of mechanical failures of the chiller(s).

Table 1. Tracer injection dates, types, and recovery locations.

Tracer Injection Date	Tracers	Detected at wells	Tracer Injection Date	Tracers	Detected at wells
October 24, 2018	DNAs*	Not available	May 1, 2019	C-Dots	PI, PB, OT, PDT
October 25, 2018	DNAs*	Not available	May 7, 2019	Phenyl Acetate	PI, OT, PDT
October 26, 2018	C-Dots	E1-PI/PB ⁰ , E1-OT	May 9, 2019	Phenyl Acetate	PI, PB, OT, PDT
October 31, 2018	C-Dots [#]	PI, PB, OT	May 21, 2019	Phenyl Acetate	PI, PB, PDT
November 1, 2018	C-Dots [#]	PI, PB, OT	July 24, 2019	Phenyl Acetate	PI, PB, PDT
November 7, 2018	C-Dots	PI, PB, OT		C-Dots	PI, OT, PB, PST, PDT
November 8, 2018	C-Dots ^ψ	PI, PB, OT		Cl, Br, K	PI, PB, PBT
November 9, 2018	Rhodamine-B	PI, OT	October 22, 2019	Phenyl Acetate	PI, PB, PDT
	Chloride	PI, OT		C-dots	PI, PB, PDT
November 14, 2018	C-Dots	PI, PB, OT		Cl, Br, K*	Not yet available
April 25, 2019	C-Dots	PI, PB, OT, E1-PST, E1-PDT, Weep near P	November 19, 2019	Rhodamine-B	PI, PB
April 29, 2019	Rhodamine-B	PI, PB, OT, PDT		Cl, Br, K*	Not yet available

*Data currently not available. [#]DNAs, CsI, LiBr included in the tracer cocktail but their recovery data not available. ^ψCsI, LiBr included in the tracer cocktail but their recovery data not available. ⁰E1-PI and E1-PB are E1-P interval and E1-P below lower packer, respectively.

Tracer injection mechanisms evolved over the course of the flow test (Mattson et al., 2019a). During early tracer tests (i.e., the October 2018 tests), a large volume of relatively low-strength tracer solution was injected using Quizix pump. This injection mechanism was modified by directly pulling a higher strength tracer solution into one of the cylinders of the Quizix pump or pulling the tracer solution in the injection line hose (October to November 2018). Finally, a dedicated ISCO pump was installed and used to push tracer solution directly into the main injection flow line (November 8 2018 to November 19, 2019). Except the early October 2018 tests, a 5-min injection pulse of 100 mL high-strength tracer solution was transmitted at a rate of 20 mL/min into the main flow line. Immediately after

injection of tracer solution, 100 mL of clean water was injected with the same injection mechanism (20 mL/min) as chase water. During the tracer and chase water injection period, the main injection flow rate was 420 mL/min. However, the chase water was not injected during the last two tracer tests (October 22, 2019 and November 19, 2019). In these tests, the ISCO cylinder was rinsed and the rinse water was collected analyzed for tracer that got stuck in the ISCO pump cylinder and connecting tubes, and the mass was used in tracer injection-recovery mass balance calculations.

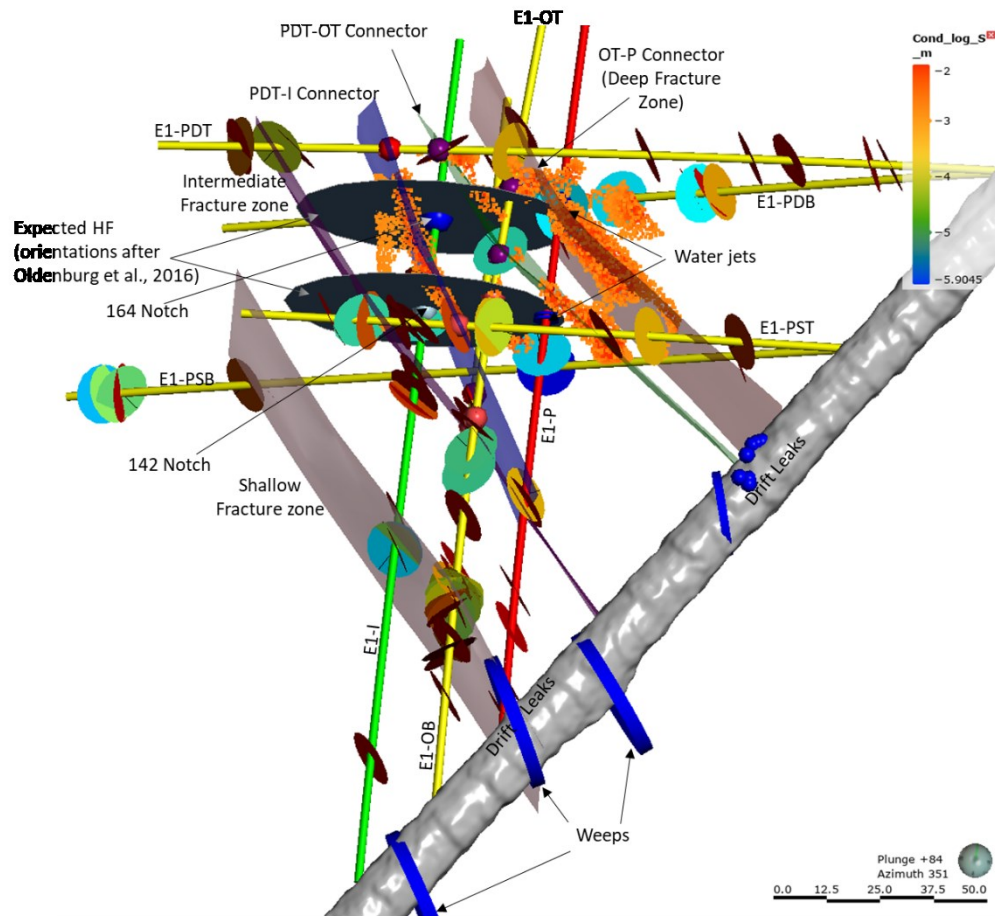


Figure 2. Natural fracture zones (or weeps) in the testbed. At least five fracture zones or weeps are identified in the testbed. Large purple spheres are temperature anomalies noticed during 164-notch activities (stimulation and flow tests) whereas large red spheres are temperature anomalies noticed during 142-notch activities (stimulation and flow tests) or entire whole pressurization after 142-notch stimulation. OT-P Connector and PDT-OT Connector are two natural fracture zones that were activated by the 164-notch activities. Borehole represented by green line (E1-I) is injection/stimulation well, red line (E1-P) is production well, and yellow lines (E1-OT/OB, E1-PST/PSB, E1-PDT/PDB) are monitoring boreholes. Baseline ERT data from Johnson et al., (2019).

3.3 Tracer Cocktail

A suite of tracer compounds, including both conservative and sorbing tracers, was used for the tracer work in the testbed. Earlier tests also included different strains of synthetic DNA; however, use of synthetic DNA was discontinued in later tests. In general, all tracer cocktail solutions were prepared in such a way that it should include at least one fluorescing tracer for near-real time detection in the drift. We used, rhodamine-B, fluorescein, C-dot, and phenol acetate as fluorescing tracers. The ability to detect tracer in the drift not only provided real-time analysis of the tracer breakthrough data at multiple producers but also helped modify sampling strategy (e.g., set/change sampling frequency, preference for overnight sampling) as well as modifying the experiment operation in real-time.

Rhodamine-B and fluorescein are widely used traditional tracers to characterize subsurface flow and hydrogeological parameters whereas the C-dot is used as a novel but non-standard was considered to be a conservative tracer. The C-dot is nanoparticle (3-5 nm in diameter) tracer consists of a carbon core decorated with a highly fluorescent polymer. Previously, C-dot is used in a few instances for subsurface fracture characterization (e.g., Hawkins, 2016). The phenol acetate was used as a thermally degrading tracer, with phenol as a degrading product. In many tracer tests, the tracer cocktails also included solute tracers such as Cl, Br, and K (Table 1).

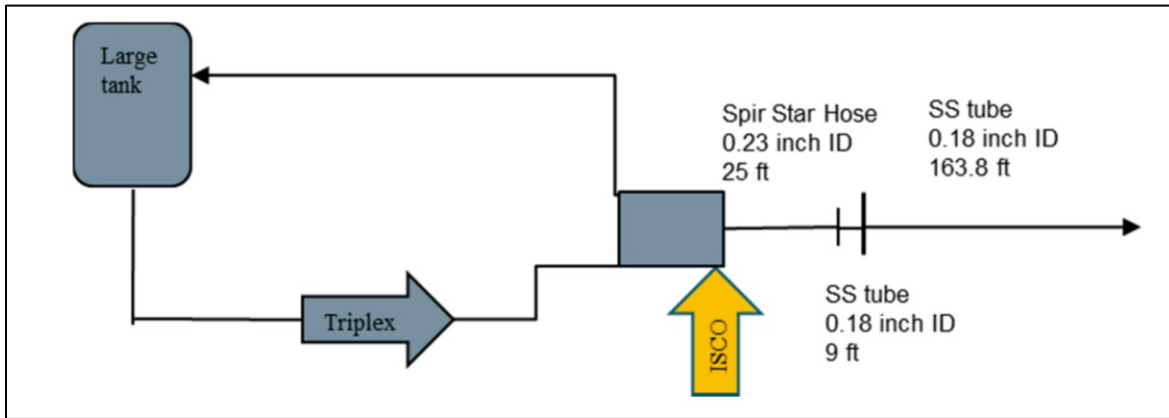


Figure 3. Schematic diagrams showing the tracer injection input for the 2019 tracer injections (adapted from Mattson et al., 2019a).

Table 2. Injection and out flow rates of producers during the 2019 tracer tests.

	In/Out flow rates (mL/min)									
	2019									
	25-Apr	29-Apr	1-May	7-May	9-May	21-May	24-Jul	22-Oct	19-Nov	
Injection rate	400	400	400	400	400	400	400	400	400	
PI Flow rate	110	110	110	142	152	120	202	215	256	
PB Flow rate	32	32	32	49	61	40	74	120	50	
OT Flow rate	3	3	3	4	3	3	2	1	1	
PST	21	21	21	17	16	20	28	5	18	
PSB	0	0	0	0	0	0	0	1	0	
PDT	97	97	97	103	98	60	27	12	20	
PDB	0	0	0	0	0	0	0	2	0	
OB	0	0	0	0	0	0	0	0	0	
Weep near P	40	40	40	40	40	40	15	15	10	
Injection_collar								21	19	

3.4 Sample Collection

Immediately after injection of tracer solution, a high frequency samples were collected from major producers (Table 2). The E1-P (the production well) below lower packer (PB) and E1-P interval (PI) flowed consistently during all tracer tests and were sampled for tracer recovery. However, some leaky monitoring wells (e.g., E1-OT, E1-PST, and E1-PDT) flowed intermittently. For example, E1-OT leak was significant during the 2018 tests and repairs made at the end of 2018 fixed this issue such that OT flow was not significant during the 2019 tests. All producers with significant flow were regularly sampled and analyzed for tracer recovery.

We adopted two methods to collect liquid samples from producers for analyses. The first method was manually collecting ‘grab’ samples in 10 mL amber sampling tubes. Typically, these samples were collected in less than a minute each, capped, labeled with the collection location and sampling time. Immediately after collection of each sample, the fluorescing tracer included in that particular tracer injection cocktail was analyzed in the drift. When phenol acetate was also included in the tracer cocktail solution along with C-dot, the analysis of thermally degrading (also kinetically controlled) product (e.g., phenol) was given preference for immediate analysis and the co-injected C-dot was analyzed later. The second method of sampling was using fraction collectors to collect samples from the three locations. The fraction collectors were set to advance at a set time interval and a peristaltic pump was used to control the rate of sampling such that the 10 ml sampling tube would be filled during the sampling interval. Unlike the grab samples, which represent a sample concentration at the moment of sampling, the fraction collector samples represent an integrated sample concentration over the sampling interval.

3.5 Tracer Analysis

All fluorescing tracers [C-dots, fluorescein, rhodamine-B, and phenyl acetate (phenol as degrading product)] were analyzed using an Ocean Optic spectrophotometer system (Ocean optic FIA-SMA-FL-UTL cell, PX-2 pulsed xenon lamp, QEPRO spectrophotometer). For each fluorescing tracer, the optimum excitation and emission radiation wavelength was identified with a tracer solution prepared in background water (pre-tracer injection PI water). Table 3 lists the excitation and emission wavelengths. For each sample, three scans average fluorescence count was recorded with 5 to 30 sec as integration time for each scan. Background fluorescence values were

established for each producer and corrected either during analysis (for PI samples) or subsequently during data processing. Prior to each analysis, a series of calibration standard solutions of the target analyte were prepared using the background (PI) water for construction of calibration curve. Consequently, the recorded fluorescence count of each sample was converted to tracer concentration using the relationship between fluorescence counts and concentration as illustrated in Figure 4.

Table 3. Excitation and Emission wavelengths

Tracer	Excitation, nm	Emission, nm
C-dots	361	468
Fluorescein	492	513
Rhodamine-B	510	582
Phenol	267	297

For solute tracers (Cl, Br, K, etc.), all time-stamped samples were shipped to laboratory for analysis with ion chromatography (IC) and inductively coupled plasma optical emission spectroscopy (ICP-OES). Some of the samples were analyzed at the Center for Advanced Energy Studies (CAES) in Idaho Falls, ID whereas some additional samples are currently being analyzed at LLNL in Livermore, CA.

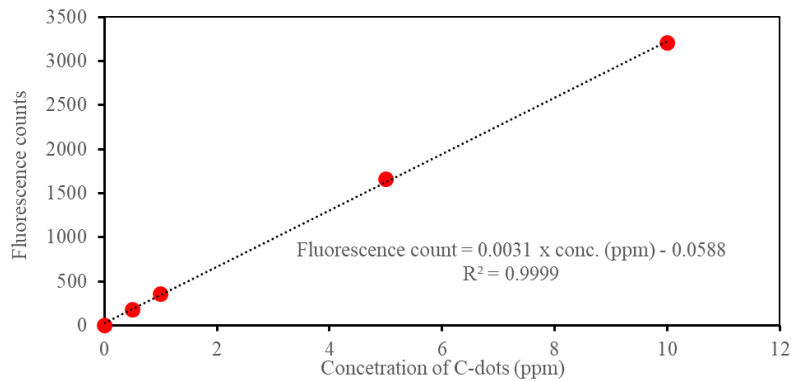


Figure 4. C-dots calibration curve constructed for July 24, 2019 tracer test.

3.6 Tracer Arrival Time Adjustment

Unlike most of other field tracer tests that lasted several months to years to complete (injection to recovery), initial tracer detection at the production wells at EGS Collab testbed occurred in less than an hour. Such short duration test made us to account all possible time delays associated with the injection and sampling. Universally for tracer tests and producers, one common time delay was the time taken by tracer pulse to get to the injection point (164-notch interval). Given the flow rate (400 mL/min) and length of the tube from drift to the injection target, we found this time delay is about 3 min. Similarly, we also figured out the travel time for water from where it left the rock/fracture and entered the outflow drain tubes at depths (e.g., for PB and PI) to the sampling location on the drift. Since the out-flow rates of both PB and PI varied over time, the time delays for PB and PI samples were different for different tests. For PB and PI, the out bound time delays ranged about 9 to 32 min and 6 to 65 min, respectively, and we adjusted respective time delays for each sample from each test. On the other hand, for outflowing monitoring wells (e.g., E1-OT, E1-PDT, E1-PST, etc.) the out-bound time delays were unknown (water travelled through the grouted hole with unknown flow channel length/volume) and such time delays were not adjusted. Finally, when fraction collector was used to collect samples, the time delays associated with the travel time for water from the producer outlet to the drip point was also adjusted in the reported time. Unlike the grab sample with instantaneous sampling an associated time stamp time, fraction collector collected water sample over a duration (mostly, in 20 min duration). For these samples, a mid-interval time stamp was used as sampling time.

4. RESULTS AND DISCUSSION

Much of the tracer characterization work of 2019 was to characterize changes in the fracture network due to the injection of water that was colder than the initial rock temperature. The chilled water experiment, started May 8, 2019 (10:15 MDT, 17:15 UTC) with the circulation of chilled water through the down-borehole heat exchanger within E1-I, cooling the temperature of the water injected into the hydraulic fracture at the 164' (50 m) notch for over 7 months of nearly uninterrupted circulation. Outside of system outages, the chilled water injection rate was maintained at 400 ml/min. Throughout this experiment a straddle packer was located over the intersection of the OT-P Connector fracture and E1-P at a depth of 121.75 ft (37.1 m) from the borehole collar, allowing for the recovery of water from the region with the straddle packer interval (E1-PI) and below the interval (E1-PB), where the hydraulic fracture intersects the E1-P borehole. Water recovery was recorded during the chilled water experiment. Water flows from all of the metered

locations were noted throughout the course of the chilled water experiment (Figure 5). At the beginning of the cold-water injection, water production was dominated by PI and PDT. During the cold-water injection, water production increased in PI and PB and decreased in PDT. Near the end of the experiment water production was predominately from E1-PB and E1-PI (> 80%), with small amounts from E1-PST and E1-PDT. Volumetric recovery from all the producing zones approached 98% near the end of the experiment (White and Fu, 2020).

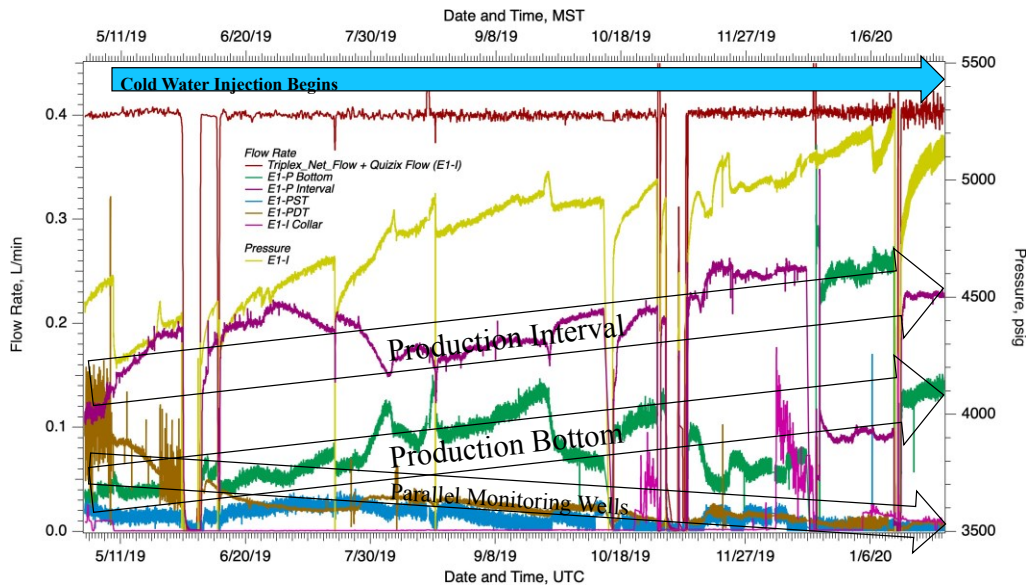


Figure 5. Injection pressure and rate, and production rates during the cold-water injection test (modified figure from Mark White, PNNL).

4.1 The Steady State Assumption

Tracer break through curves for the April 25th, May 1st (prior to thermal injection), July 24th and October 22nd are plotted in Figure 6 for wells PI, PB, and PDT as a function of volume of water produced during each trace test. Plotting the C-dot concentration normalized to the injection concentration as a function of volume is more appropriate since the water recovery rate for each production location changed during this 7-month period. The tracer initial arrival and peak concentration as a function of produced water volume (Table 4) do not exhibit a consistent trend with time during the cold-water injection test. This is believed to be partially due the dynamic nature of the fracture system in response to the injection pressure potential changing flow pathways during this test. During this time, numerous sharp pressure drops were noted in the injection pressure (see yellow line and red dots in Figure 7) which is believed to represent the creation of new fractures as the injection pressure reached a critical value. These new fractures appear to affect the production rates, both positively and negatively, of the two main production zones (PI and PB) and to a lesser extent PDT.

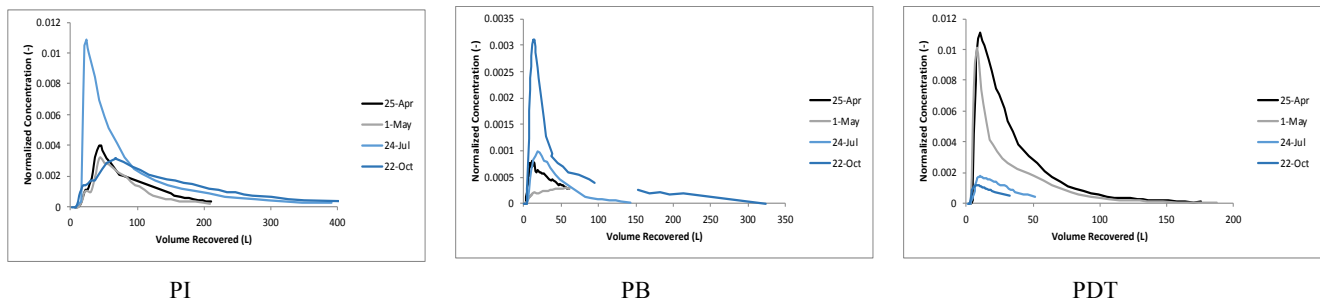


Figure 6. C-dot tracer break through curves plotted for PI, PB, and PDT

Table 4. Volume of produced water (L) for the initial detection of the C-dot tracer and the peak concentration for PI, PB, OT and PDT.

Date	Tracers	PI		PB		OT		PDT	
		First	Peak	First	Peak	First	Peak	First	Peak
April 25, 2019	C-Dots	10.1	45.5	3.7	11.0	0.3	0.7	4.0	10.2
May 1, 2019	C-Dots	13.6	44.3	2.1	56.8	0.3	0.9	3.7	7.8
July 24, 2019	C-Dots	15.9	24.2	4.9	18.2	0.4	0.6	3.7	10.1
October 22, 2019	C-dots	9.9	66.3	5.0	12.4	NA	NA	3.2	7.4

Although there are overall positive and negative produced water rate changes over the duration of the cold-water injection (see Figure 5), the numerous injection pressure drops (symbolized by the red dots in Figure 7) are frequent enough such that individual production wells experience several episodic increases and decreases in their water production between tracer tests (represented by the red vertical lines in Figure 7). As a result, comparison of individual tracer tests becomes much more complicated and the changes seen in the tracer break through curves (Table 4) are both due to the creation/change of fractures by pressure as well as the injection of cold-water creating thermoelastic effects.

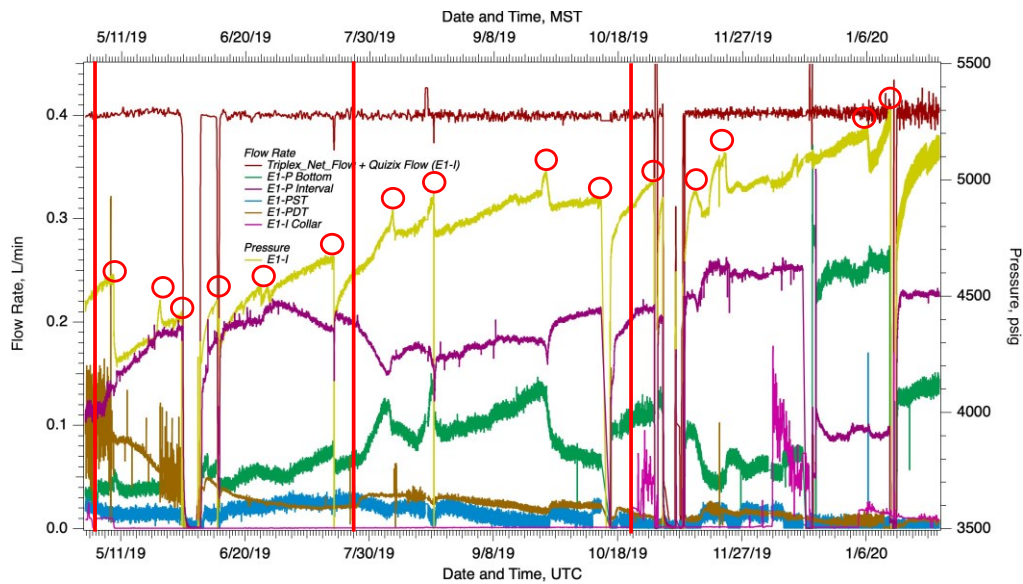


Figure 7. Injection pressure perturbations and resulting produced water flow rate changes as a function of time. Red vertical lines indicate time when a C-dot tracer injection test was performed (modified figure from Mark White, PNNL).

4.2 Tracer Recovery Mass-Balance

Nine tracer tests were conducted during the cold-water injection test up to November 19, 2019. Two additional tracer tests have been conducted in January 2020. April through July tests included a 100 ml “chase” clean water injection in an attempt to clean the pump and injection lines of residual tracer. October and November tests did not use the chase water injection protocol and instead back-flushed the injection line and pump into a graduated cylinder to record the volume and measure the tracer concentration, allowing for an adjustment of the tracer mass injected. Subsequent analysis of the tracer in the back flushed water suggest that 10 to 20% can be trapped in injection lines and injection pump. It is not certain that a 100 ml chase water flush will inject this residual tracer into the injection interval. It is the authors’ opinion that the back-flushing method produces a better pulse input than the chase water method.

Table 5 lists the tracer mass balance and water mass balance for each of the production wells. Whereas greater than 75% of the injected water is consistently recovered from the production zones, only approximately 33% of the tracer is recovered with this produced water. Several reasons could account for this discrepancy: 1) The tracer mass is calculated from the tracer break through curves which do not encompass the complete concentration vs volume curve thereby biasing the calculated tracer mass. 2) Delayed tracer break throughs after sampling is complete are not accounted in the total tracer mass recovery. 3) Water is recovered in the production wells that did not originate from the injection well. 4) The tracer is irreversible absorbed or filtered in the system.

Table 5. Tracer mass balance calculated from integration of break through curves and water mass balance calculated from flow rate. Both values are expressed as a percent of mass of tracer injected and injection flow rate.

Date	Tracer/water	PI	PB	OT	PST	PSB	PDT	PDB	OB	Weep	Total
April 25, 2019	C-Dots	13.5	1.3	0.5	1.3	0.0	17.5	0.0	0.0	2.6	36.7
	Water	27.5	8.0	0.8	5.3	0.0	24.3	0.0	0.0	10.0	75.8
May 1, 2019	C-Dots	10.7	0.6	0.2	0.0	0.0	11.1	0.0	0.0	0.0	22.6
	Water	27.5	8.0	0.8	5.3	0.0	24.3	0.0	0.0	10.0	75.8
July 24, 2019	C-dots	32.6	2.1	0.3	0.6	0.0	2.3	0.0	0.0	0.0	37.9
	Water	50.5	18.4	0.4	6.9	0.0	6.6	0.0	0.0	3.8	86.6
Oct. 22, 2019	C-dots	26.8	6.4	0.0	0.0	0.0	1.2	0.0	0.0	0.0	34.4
	Water	53.8	30.0	0.2	1.3	0.3	3.0	0.5	0.0	3.8	98.0

The magnitude of incomplete break through curves can be investigated by fitting equations to the tracer concentration vs volume data and re-calculating the mass balance. Sampling for longer periods of time can assess delayed break through due to longer pathways. Distinguishing between the collection of non-tracer laden water and filtering/decay/absorption is somewhat harder.

Figure 8 represents a method to determine the source of water produced at the three major water producing zones (PI, PB and PDT) during the long-term cooling test. In this plot, the percent of C-dot mass recovered normalized to the total injected mass is plotted against the percent of water recovered normalized to the injection flow rate. As seen in the figure, the percent of tracer recovered to the percent of water produced of all three wells exhibit a linear relationship. The linear relationship between tracer recovery and water recovery can be interpreted to support two conceptual models. The first model assumes a constant inflow of water that does not include tracer. In this case, the remaining water would have a tracer concentration percent equal to the slope of the linear regression seen in Figure 8. The second conceptual model assumes that the inflow of non-tracer water is proportional to that of the regression slope and the inflow of tracer water is at a concentration ratio of one. The two conceptual models cannot be distinguished from one another with only this data.

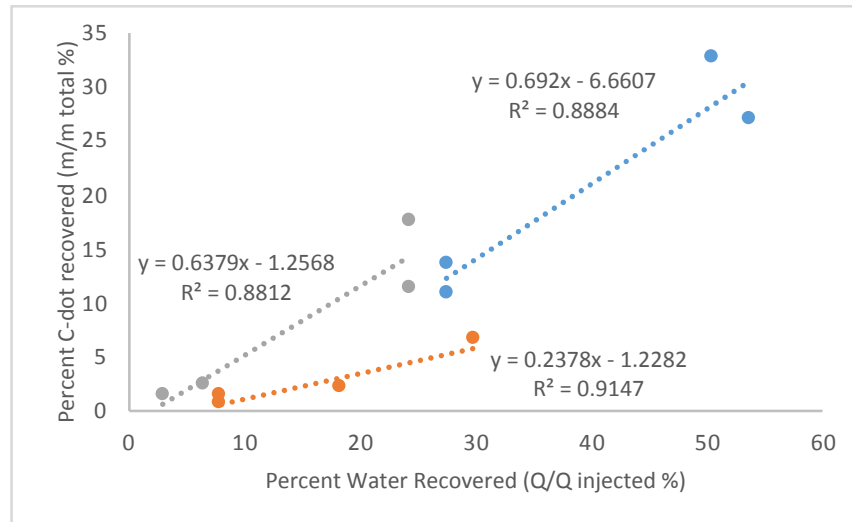


Figure 8. Plot comparing the percent by mass of C-dot recovered of the initial injection mass to the percent of water recovered by flow rate to the injection rate (blue data = PI, orange data = PB, and grey data = PDT).

Examining the produced water electrical conductivity as a function of flow rate may provide additional information to distinguish between the two conceptual models described in the previous paragraphs. If the non-tracer water is proportional to the tracer laden water, then the electrical conductivity should be a constant regardless of the flow rate. If the non-tracer water is a constant (or near constant) and the flow rate is controlled by the tracer laden water, then the conductivity should change as a function of the flow rate. For

this field experiment, the injected water has a conductivity of approximately 490 uS/m (measured on 01/28/2020) whereas the non-tracer water is believed to be higher. The plot of electrical conductivity vs flow rate for PI (see Figure 9) suggests the electrical conductivity of the PI produced water decreases with increasing flow rate. A mixing cell model (Equation 1) fit of the day which optimizes the background water electrical conductivity and inflow rate suggest the following data; non-tracer water electrical conductivity 2000 mS/m with a flow rate equal to 27 ml/min. These values appear to be fairly reasonable to what we might expect in the field. The regression intercept of Figure 8 would intersect zero tracer concentration at approximately 52 ml/min of input of non-tracer water. Based on these results we can consider that input of non-tracer water to nearly be a constant, however, it is likely that this input is not a complete constant but exhibits a small amount of variability as a function of flow rate.

The mixing equation is express as:

$$EC_{total} = \frac{EC_{inj} * Q_{inj} + EC_{bkgn} * Q_{bkgn}}{Q_{total}} \tag{Equation 1.}$$

where EC_{total} is the measured electrical conductivity, EC_{inj} is the injection water electrical conductivity, Q_{inj} is the injection rate, EC_{bkgn} is the non-tracer water electrical conductivity, Q_{bkgn} is the fitted non-tracer flow rate, and Q_{total} is the measured production rate.

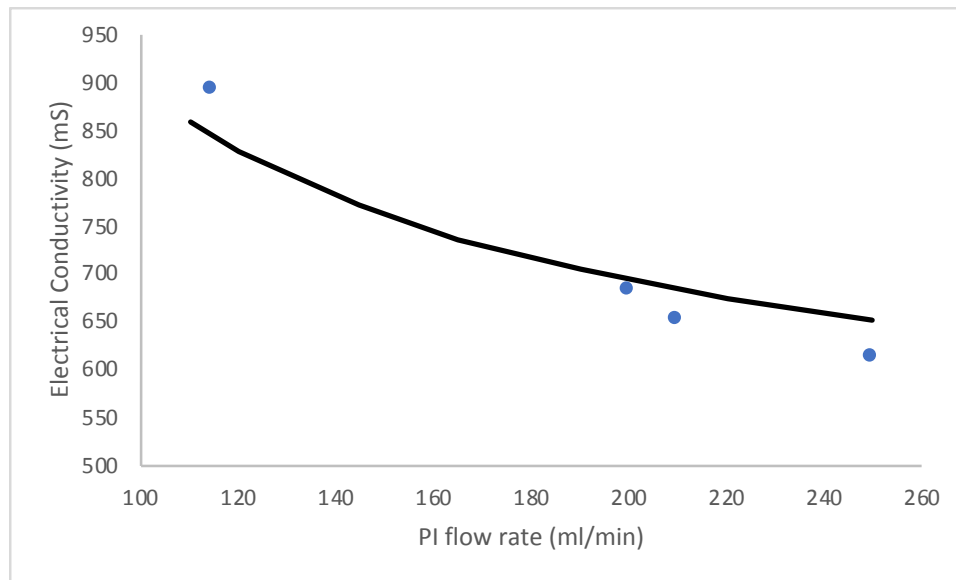


Figure 9. Plot of the production well interval flow rate as a function of the produced water electrical conductivity.

Recent sorption isotherm tests results suggest that C-dots do not behave as a conservative tracer and exhibit a Langmuir type sorption to crushed Poorman Formation rocks. It is unknown at this time if this sorption is irreversible.

Based on geophysical monitoring, fiber optic temperature measurements, water flow production response, core descriptions and well bore analyses, a simple flow conceptual model of the flow to the three dominate producing wells is illustrated in Figure 10. Injected water is believed to be flowing from the 164-notch through a single (or multiple) fracture(s) towards the production well. Some of the injected water (3 to 7%) is diverted to the PDT well via a natural fracture and then the water travels through a grout filled borehole to the drift. The pressure at the intersection of the natural fracture and the PDT borehole is not known. The majority of the injected water (70 to 84%) continues through the hydraulic fracture until it bifurcates into two pathways. One pathway is along the hydraulic fracture that continues to intersect the production well below the lower packer (PB). The other water pathway flows through a second natural fracture to the production well between the packers (PI). For both these production zones, water is transmitted to the drift through ¼ inch stainless steel tubing resulting in a well pressure near atmospheric pressure. Certainly, the flow pathways are more complicated than this simple conceptual model but the model provides an easy layout of the water flow pathways that can explain most of the flow and tracer behavior.

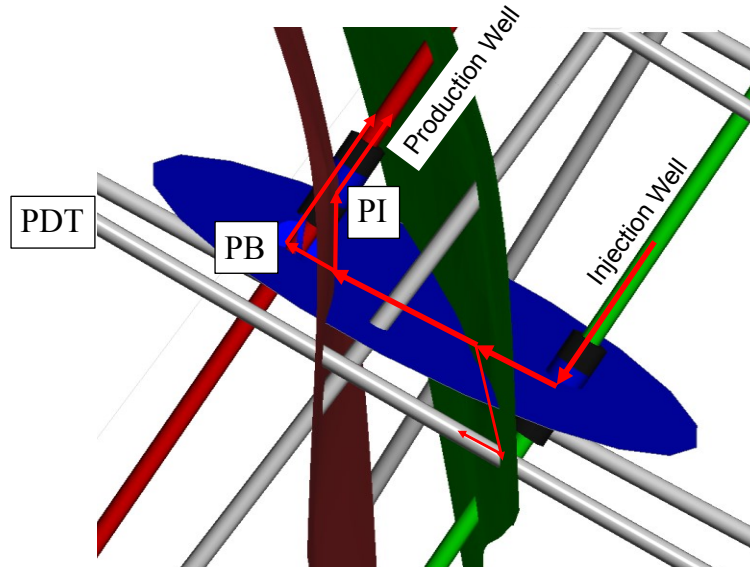


Figure 10. Major outflows patterns observed during July 24, October 22, and November 19 tracer tests.

5. SUMMARY

Both fracture cooling and pressure perturbations appear to have affected the fracture flow pathways of the Experiment 1 test bed during the cold-water test. Overall the water production rate of the two production well zones have significantly increased during this time (Figure 5). However, the increase has not always been constant and due to sudden injection well pressure decreases, water produced from these two locations have exhibited temporary decreases in the water production rate (see Figure 7).

PDT seems to be minimally affected by these changes during this test (see Table 4). One interpretation is that the lack of changes in the PDT tracer's first and peak arrival volume parameters, despite 7 months of cold-water injection and numerous pressure step changes, suggest that any changes to the fracture system are not near injection well hydraulic fracture and the natural fracture leading to PDT.

PI and PB water production rates appear to be generally inversely correlated (see Figure 7) and likely share a common flow pathway from the injection well. Although there is an overall increase in both PI and PB water production rates during the 7-month test, the two production zones compete for the same injected water.

Analysis of the C-dot recovery vs water recovery for the three main production zones suggest that there exists a linear relationship between the two parameters (see Figure 8). This linear relationship could be due to a constant input of non-tracer laden water where any change in the total flow rate is due to injected tracer laden water that exhibits some tracer mass lost (e.g. irreversible absorption, filtering, degradation). A second model that would support this linear relationship is that there is no loss of tracer mass in the injected water recovery and any change in the total production rate is due to proportional rate changes in the tracer and non-tracer laden produced water. Examining the electrical conductivity vs flow rate for the PI production zone suggests the first hypothesis is correct.

A simplified fracture conceptual model has to be constructed illustrating potential flow pathways based on geophysical, temperature changes, borehole and core studies. These flow pathways can be used to better interpret the flow rate and tracer break through curves at the various production zones.

ACKNOWLEDGEMENTS

The research supporting this work took place in whole or in part at the Sanford Underground Research Facility in Lead, South Dakota. Funding for this work is supported by the Office of Science of the Department of Energy under Contract Number DE-AC07-05ID14517 with Idaho National Laboratory. The assistance of the Sanford Underground Research Facility and its personnel in providing physical access and general logistical and technical support is acknowledged. The earth model output/visualizations for this paper were generated using Leapfrog Software. Copyright © Seequent Limited. Leapfrog and all other Seequent Limited product or service names are registered trademarks or trademarks of Seequent Limited.

REFERENCES

- Dobson, P., Kneafsey, T.J., Blankenship, D., Valladao, C., Morris, J., Knox, H., Schwering, P., White, M., Doe, T., Roggenthen, W., Mattson, E., Podgorney, R., Johnson, T., Ajo-Franklin, J., and the EGS Collab Team: An introduction to the EGS Collab project. *GRC Transactions*, **41**, (2017).
- Heise, J.: The Sanford underground research facility at Homestake. *Journal of Physics: Conference Series*, 606(1), (2015).
- Huang, H., Neupane, G., Podgorney, R., Mattson, E., & the EGS Collab Team, 2019. Mechanistically modeling of hydraulic fracture propagation and interaction with natural fractures at EGS-Collab Site. *Proceedings 44th Workshop on Geothermal Reservoir Engineering*, Stanford University, Stanford, CA, (2019).
- Johnson, T., Strickland, C., Knox, H., Thomle, J., Vermuel, V., Ulrich, C., Kneafsey, T., Blankenship, D., and EGS Collab Team: EGS Collab project electrical resistivity tomography characterization and monitoring status. *Proceedings 44th Workshop on Geothermal Reservoir Engineering*, Stanford University, Stanford, CA, (2019)
- Kneafsey, T.J. and Dobson P.F., Ajo-Franklin, J.B., Guglielmi, Y., Valladao, C.A., Blankenship, D.A., Schwering, P.C., Knox, H.A., White, M.D., Johnson, T.C., Strickland, C.E., Vermuel V.R., Morris, J.P., Fu, P., Mattson, E., Neupane, G., Podgorney, R.K., Doe, T.W., Huang, L., Frash, L.P., Ghassemi, A., Roggenthen, W., and the EGS Collab Team: EGS Collab Project: Status, Tests, and Data. ARMA-19-2004, (2019).
- Kneafsey, T.J., Blankenship, D., Dobson, P.F., Morris, J.P., White, M.D., Fu, P., Schwering, P.C., Ajo-Franklin, J.B., Huang, L., Schoenball, M., Johnson, T.C., Knox, H. A., Neupane, G., Weers, J., Horne, R., Zhang, Y., Roggenthen, R., Doe, T., Mattson, E., Valladao, C., and the EGS Collab team: The EGS Collab Project: Learnings from Experiment 1, *Proceedings 44th Workshop on Geothermal Reservoir Engineering*, Stanford University, Stanford, CA, (2020).
- Knox, H., Fu, P., Morris, J., Guglielmi, Y., Cook, P., Herrick, C., Lee, M., Ajo-Franklin, J., Su, J.C., and the SIGMA-V Team: Fracture designs for the Collab/SIGMA-V project. *GRC Transactions*, **41**, (2017).
- Mattson, E.D., Neupane, G., Plummer, M.A., Hawkins, A., Zhang, Y. and the EGS Collab Team: Preliminary Collab fracture characterization results from flow and tracer testing efforts, *Proceedings 44th Workshop on Geothermal Reservoir Engineering*, Stanford University, Stanford, CA, (2019a).
- Mattson, E.D., Neupane, G., Hawkins, A., Burghardt, J., Ingraham, M., Plummer, M., and the EGS Collab Team: Fracture Tracer Injection Response to Pressure Perturbations at an Injection Well, *GRC Transactions*, **43**, (2019).
- Moore, J., McLennan, J., Allis, R., Pankow, K., Simmons, S., Podgorney, R., Wannamaker, P., Bartley, J., Jones, C., and Rickard, W.: The Utah Frontier Observatory for Research in Geothermal Energy (FORGE): An International Laboratory for Enhanced Geothermal System Technology Development, *Proceedings*, 44th Workshop on Geothermal Reservoir Engineering, Stanford University, Stanford, CA (2019).
- Neupane, G., Podgorney, R.K., Huang, H., Mattson, E.D., Kneafsey, T.J., Dobson, P.F., Schoenball, M., Ajo-Franklin, J.B., Ulrich, C., Schwering, P.C. and Knox, H.A., Blankenship, D.A., Johnson, T.J., Strickland, C.E., Vermeul, V.R., White, M.D., Roggenthen, W., Uzunlar, N., Doe, T.W., and the EGS Collab Team: EGS Collab Earth Modeling: Integrated 3D Model of the Testbed, *GRC Transactions*, **43**, (2019).
- Oldenburg, C.M., Dobson, P.F., Wu, Y., Cook, P.J., Kneafsey, T.J., Nakagawa, S., Ulrich, C., Siler, D.L., Guglielmi, Y., Ajo-Franklin, J., Rutqvist, J., Daley, T.M., Birkholzer, J.T., Wang, H., Lord, N.E., Haimson, B.C., Sone, H., Vigilante, P., Roggenthen, W.M., Doe, T.W., Lee, M.Y., Ingraham, M., Huang, H., Mattson, E.D., Zhou, J., Johnson, T.J., Zoback, M.D., Morris, J.P., White, J.A., Johnson, P.A., Coblenz, D.D., and Heise, J.: Intermediate-Scale Hydraulic Fracturing in a Deep Mine, kISMET Project Summary 2016, Lawrence Berkeley National Laboratory, LBNL-1006444, (2016).
- Singh, A., Zoback, M., Neupane, G., Dobson, P.F., Kneafsey, T.J., Schoenball, M., Guglielmi, Y., Ulrich, C., Roggenthen, W., Uzunlar, N., Morris, J., Fu, P., Schwering, P.C., Knox, H.A., Frash, L., Doe, T.W., Wang, H., Condon, K., Johnston, B., and the EGS Collab Team, 2019. Slip Tendency Analysis of Fracture Networks to Determine Suitability of Candidate Testbeds for the EGS Collab Hydroshear Experiment. *GRC Transactions*, **43**, (2019).
- Ulrich, C., Dobson, P.F., Kneafsey, T.J., Roggenthen, W.M., Uzunlar, N., Doe, T.W., Neupane, G., Podgorney, R., Schwering, P., Frash, L. and Singh, A.: The distribution, orientation, and characteristics of natural fractures for Experiment 1 of the EGS Collab Project, Sanford Underground Research Facility. In *Proceedings, 52nd US Rock Mechanics/Geomechanics Symposium*, American Rock Mechanics Association, ARMA 18-1252, (2018).

- White, M., P. Fu, and EGS Collab Team: Application of an Embedded Fracture and Borehole Modeling Approach to the Understanding of EGS Collab Experiment 1, *Proceedings, 45th Workshop on Geothermal Reservoir Engineering*, Stanford University, Stanford, CA (2020).
- White, M., Fu, P., Huang, H., Ghassemi, A., and EGS COLLAB Team: The Role of Numerical Simulation in the Design of Stimulation and Circulation Experiments for the EGS Collab Project. *GRC Transaction*, **41**, (2017).
- White, M., T. Johnson, T. Kneafsey, D. Blankenship, P. Fu, H. Wu, A. Ghassemi, J. Lu, H. Huang, G. Neupane, C. Oldenburg, C. Doughty, B. Johnston, P. Winterfeld, R. Pollyea, R. Jayne, A. Hawkins, Y. Zhang, and EGS Collab Team: The Necessity for Iteration in the Application of Numerical Simulation to EGS: Examples from the EGS Collab Test Bed 1, *Proceedings, 44th Workshop on Geothermal Reservoir Engineering*, Stanford University, Stanford, CA (2019).
- Williams, C.F., Reed, M.J., Mariner, R.H., DeAngelo, J., and Galanis, S.P. Jr.: Assessment of moderate- and high-temperature geothermal resources of the United States. US Department of the Interior, US Geological Survey, Fact Sheet 2008-3082, (2008).